HYSCORE and DEER with an upgraded 95 GHz pulse EPR spectrometer

Daniella Goldfarb [a,*], Yaakov Lipkin [a], Alexey Potapov [a], Yehoshua Gorodetsky [a], Boris Epel [b], Arnold M. Raitsimring [c], Marina Radoul [a], Ilia Kaminker [a]

[a] Department of Chemical Physics, Weizmann Institute of Science, Rehovot 76100, Israel
[b] Department of Radiation & Cellular Oncology, MC1105, The University of Chicago Medical Center, Chicago, IL 60637, USA
[c] Department of Chemistry, University of Arizona, Tucson, AZ 85721, USA

ARTICLE INFO

ABSTRACT

The set-up of a new microwave bridge for a 95 GHz pulse EPR spectrometer is described. The virtues of the bridge are its simple and flexible design and its relatively high output power (0.7 W) that generates π pulses of 25 ns and a microwave field, $B_1 = 0.71$ mT. Such a high B_1 enhances considerably the sensitivity of high field double electron-electron resonance (DEER) measurements for distance determination, as we demonstrate on a nitroxide biradical with an interspin distance of 3.6 nm. Moreover, it allowed us to carry out HYSCORE (hyperfine sublevel-correlation) experiments at 95 GHz, observing nuclear modulation frequencies of ^{14}N and ^{17}O as high as 40 MHz. This opens a new window for the observation of relatively large hyperfine couplings, yet not resolved in the EPR spectrum, that are difficult to observe with HYSCORE carried out at conventional X-band frequencies. The correlations provided by the HYSCORE spectra are most important for signal assignment, and the improved resolution due to the two dimensional character of the experiment provides ^{14}N quadrupolar splittings.

© 2008 Elsevier Inc. All rights reserved.

1. Introduction

The scope of high field EPR is broad and, in principle, encompasses all the sub-disciplines of EPR spectroscopy, namely continuous wave (CW), time resolved and pulsed EPR, electron-nuclear-double resonance (ENDOR) and double electron-electron resonance (DEER) techniques. In the last decade numerous applications of high field CW EPR and ENDOR have been reported and the virtues of measurements at a high field have been well demonstrated and established [1–6]. Recently, it has also been demonstrated that distance measurements between paramagnetic centers by pulsed DEER techniques can also be performed at high fields [9–12]. Distance measurements have become very popular in the last few years and are carried out usually at X-band frequencies [7,8]. The high field measurements offer additional information such as the relative orientations of the g-tensors of the two coupled paramagnetic centers [10]. Among the above mentioned high resolution EPR techniques, the absence of applications of electron–spin echo modulation (ESEEM) spectroscopy is conspicuous. ESEEM spectroscopy is a well established method for measurements of small hyperfine and nuclear quadrupole interactions [13,14], and is complementary to ENDOR. The ESEEM advantages are that it does not require the application of RF (radio-frequency) pulses, and therefore it is simpler than ENDOR in terms of cavity design and hard-

ware requirements. Furthermore, a unique and most useful property of ESEEM experiments is the possibility to generate sum combination frequencies. The frequency and the fine structure of sum combination lines are directly related to the anisotropic part of the hyperfine interaction [17] and the nuclear quadrupole interaction, respectively [15,16]. Moreover, two dimensional (2D) ESEEM experiments (such as hyperfine sublevel correlation, HYSCORE, spectroscopy) can be readily performed. These experiments often yield highly resolved spectra, disentangling overlapping signals arising from multiple nuclei and providing correlations that are essential for signal assignment. These virtues turned HYSCORE spectroscopy into a very popular technique.

In the past, due to widespread use of proton related ESEEM measurements it was often assumed that ESEEM spectroscopy is best performed at low frequencies (2–9 GHz) to decrease Zeeman frequencies of nuclei and therefore facilitate the simultaneous excitation of forbidden and allowed EPR transitions necessary for the generation of the ESEEM effect. This led to the design and construction of low frequency pulse EPR spectrometers such as S- and C-band spectrometers [18–22]. However, experience with Ku, (12–18 GHz) Ka- and Q-band (26–35 GHz) gained during the last few years showed that ESEEM spectroscopy at these frequencies can be routine and very useful [23–25], thus expanding considerably the range of multi-frequency ESEEM. We expect that ESEEM experiments carried out at even higher frequencies will make new ranges of hyperfine and nuclear quadrupole couplings accessible. This is supported by a few reports of ^{14}N ESEEM observed at W-

band, where the hyperfine couplings were on the order of the nuclear Zeeman frequency [26–28]. In these reports, however, the frequencies observed were below 10 MHz, corresponding to the electron–spin manifold for which the hyperfine coupling and the Larmor frequency are of opposite signs. The nuclear frequencies of the second electron–spin manifold, which are higher, could not be observed due to power (B_1) limitations. Nonetheless, these reports, along with the new pulse sequences designed for the enhancement of the nuclear modulation [29–31], call for implementing ESEEM spectroscopy at W-band (95 GHz).

As mentioned above, the major obstacle for the observation of nuclear modulation at high operational frequencies is the lack of the mw (microwave) power necessary to produce mw pulses with a large enough bandwidth and amplitude that can excite simultaneously the relevant allowed ($\Delta M_S = \pm 1$, $\Delta M_I = 0$) and forbidden ($\Delta M_S = \pm 1$, $\Delta M_I \neq 0$) electron–spin transitions. At lower operational frequencies (2–34 GHz) the problem was solved by introducing high power amplifiers and constructing specially designed cavities. Unfortunately, the available power of commercial W-band spectrometers generates a B_1 amplitude of only ~0.28 mT ($\omega_1 \sim 8$ MHz) [12]. This limits the number of systems amenable for ESEEM investigations. The limited B_1 also restricts W-band DEER applications. The DEER experiment, in principle, does not require very short pulses, but the pulse bandwidth does determine the upper limit of the dipolar interaction that can be accessed by the technique. Moreover, insufficient mw power requires the application of relatively long pulses (~100 ns) [12] and thereby reduces the sensitivity of the technique.

The first homebuilt pulsed W-band EPR spectrometers were based on Ukrainian technology, using IMPATT amplifiers and the maximum output power of the W-band microwave bridge was about 200–250 mW, producing π pulses with a minimum length of 80 ns [32–34,28]. This is higher or comparable to the power available in most commercial W-band spectrometers [12]. A pulse EPR spectrometer, operating at 140 GHz, utilizing a 300 W extended interaction klystron reported a $\pi/2$ pulse duration of ~14 ns with full power that was estimated as 30 W incident on a Fabry-Perot cavity [35]. Recently, a unique high power W-band spectrometer has been reported by Freed and coworkers [36]. It's high mw power (1 kW) originate again from a specialized mm-wave amplifier tube, an extended interaction klystron. This spectrometer features pulses of 5 ns with a spectral width of 200 MHz and a deadtime of about 50 ns. This particular spectrometer was specifically designed for Fourier transform (FT) EPR measurements at ambient temperatures. It is primarily used for the investigation of the dynamics of complex systems of biological relevance in aqueous solutions, where the paramagnetic entity is usually a nitroxide spin probe. This spectrometer employs quasioptical techniques in the high-power stages to reduce power losses and a compact Fabry-Pérot resonator. In principle, such a spectrometer could be duplicated and accommodated for low temperature ESEEM/DEER measurements, but due to the uniqueness of the mw source this idea is impractical. A more practical approach is to upgrade the design of the old W-band bridge, taking advantage of the progress made in the last decade in the development of commercially available mw components.

Here we present a new W-band bridge with a relatively high power, constructed from available commercial components, based on waveguide technology. It is designed primarily for low temperature electron spin echo spectroscopy that require the application of short powerful mw pulses, such as ESEEM and DEER. The virtues of this bridge are its simple design and flexibility, which makes any modification straightforward. It has an output power of 0.7 W with long term power and phase stability and it features a π pulse of 25 ns. This new W-band bridge replaced our old microwave bridge, which had a maximum power of 250 mW, obtained using IMPATT amplifier technology [24].

In the following we describe the new bridge and some other minor changes made to our homebuilt spectrometer. The spectrometer performance is demonstrated on DEER measurements of a rigid nitroxide biradical and on HYSCORE measurements of two systems in frozen solutions. The first is the NO complex of ferrous myoglobin, revealing ^{14}N frequencies and resolving quadrupolar splittings, and the second is $V^{17}O(H_2^{17}O)_5^{2+}$ showing ^{17}O frequencies. The range of nuclear frequencies observed is 8–40 MHz, demonstrating the potential of such measurements for deciphering transition metal coordination spheres in a variety of systems.

2. The MW bridge

The design of the mw bridge is simple and similar to standard pulse X-band spectrometers. Except for the source, all operations, such as pulse formation and phase modulation are carried out at 95 GHz. The bridge utilizes a homodyne detection scheme, without the involvement of an intermediate frequency. The scheme of the bridge is given in Fig. 1. It consists of two identical channels, each of which can generate pulses with controlled independent frequency, phase and amplitude. Channel I uses a computer controlled frequency synthesizer (7.3 ± 0.1 GHz, with a frequency step of 1 kHz, Herley, CTI XS-7311). The source output is amplified to produce 20 mW power that is fed into a x13 multiplier followed by a bandpass filter, producing a 94.9 ± 1.3 GHz continuous wave signal. Part of this signal is directed, via a 3 dB directional coupler, to the receiver arm and the other part passes through a narrow band isolator that suppresses possible leakage of a reflected amplified signal to the reference arm. The signal is then fed into a digital phase modulator (0/180°) and to a fast PIN switch to form pulses. The output pulses are then preamplified and fed into a voltage controlled variable PIN attenuator for power adjustment.

Channel II is similar to channel I and has a manual phase shifter for adjusting the relative phase of the two channels. At the moment it lacks a digital phase modulator that will be installed in the near future. The current source of the second channel is based on a ADF4113 chip (BA Microwave, 0.4–8 GHz, resolution of 20 kHz). This will be replaced shortly with a source similar to channel I. The sources of the two channels are not commonly locked, but with a fast switch (Eyal microwaves, 35 ns switching speed) and a splitter it is possible to connect channel II to the source of channel I. The pulses formed in the two different channels are combined using a 3 dB directional coupler and then amplified by a gated 23 dB solid state amplifier with a saturated power output (P_s) of 1 W. The amplified pulses pass through a mechanical attenuator for further adjustment of the output power. The pulses are finally fed into the cavity via a circulator. The maximum power available at the output of the circulator is 700 mW. The probehead houses a cylindrical TE_{011} cavity and has been described previously [34]. Due to losses in the waveguide leading to the cavity, the power at the entrance to the cavity is 300–350 mW.

The transient signals reflected from the cavity are fed into the receiver, which consists of a 20 dB directional coupler connected to a diode detector for viewing the reflected pulses from the cavity for diagnostic and tuning purposes. The main power then goes through a protect PIN switch, similar to those used in channel I and II for pulse forming, a variable mechanical attenuation, a low noise amplifier (LNA) and a mixer. The LO (local oscillator) input of the mixer comes from channel I. To adjust the phase of the receiver and to optimize the LO power level needed for the best mixer response, the input power passes through a mechanical variable attenuator, a 20 dB power amplifier, a 6 dB fixed attenuator and a mechanical phase shifter. The video signal (IF output of the mixer) is preamplified by a broadband video amplifier (0–500 MHz) and is directed to the acquisition system of the spectrometer via
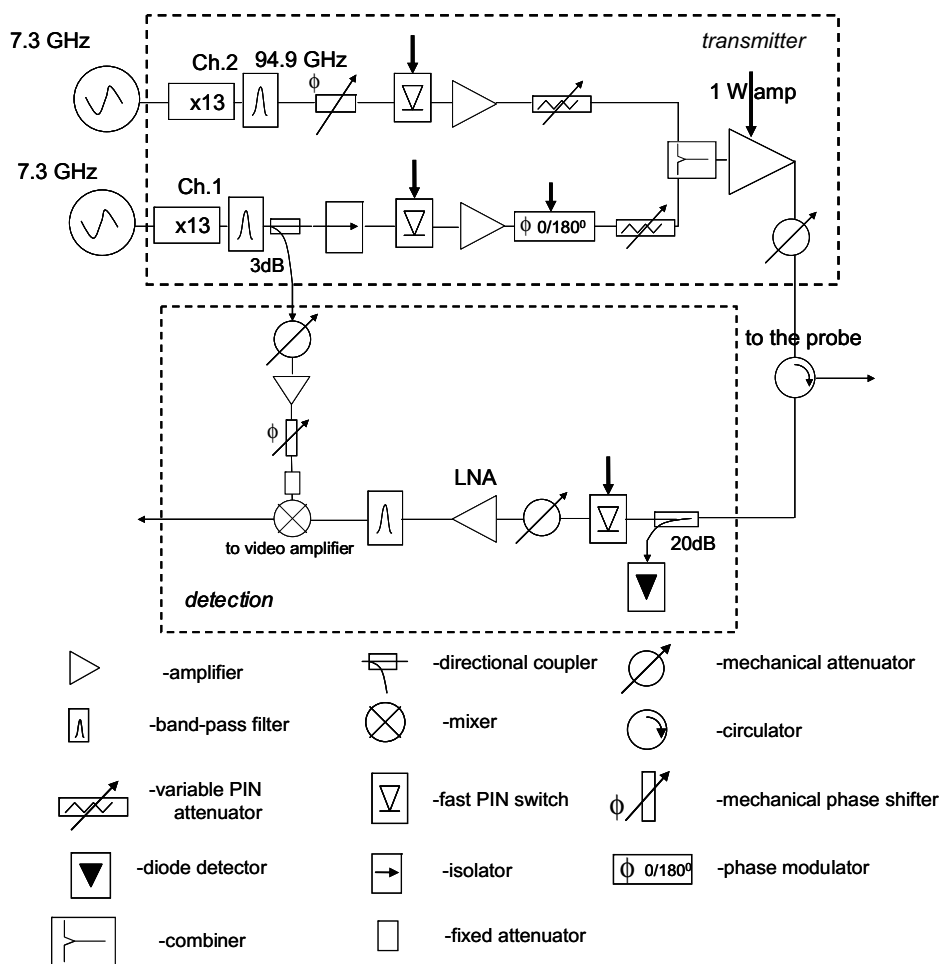
Fig. 1. A schematic diagram of the W-band bridge. The bold arrows mark digitally controlled components.

a 0–95 MHz filter. The total gain of the receiver, taking into account the amplification of the LNA and the video amplifier, and the losses of the mixer, PIN switch and directional coupler, is 31.6 dB.

Table 1 lists the microwave components and their most relevant specifications. The operational frequency of the bridge is 95 ± 0.25 GHz and its bandwidth is determined by the components with the lowest bandwidth, which currently are the frequency multiplier and the phase modulator.

3. The pulse programmer and the software control

The original pulse programmer of the spectrometer (RS690, Interface Technology) had a time resolution of 4 ns and a large enough number of channels, but it suffered from a slow reprogramming time (∼50 ms). This is not a major problem for ENDOR experiments, where the variable experimental parameter is the RF and phase cycling can be accommodated per scan rather than per point, but it is a considerable handicap for ESEEM type of experiments where time intervals are continuously varied. This is particularly crucial for two dimensional experiments such as HYSCORE, where two time intervals are varied. This low reprogramming rate can actually double or even triple the duration of a HYSCORE experiment and therefore the old pulse programmer has been replaced with a PulseBlasterPro (Spincore) PCI card. The latter has a resolution of 2.5 ns and a reprogramming time of ∼67 μs per instruction. For a HYSCORE experiment, that includes around 20 operations, this amounts to 1.3 ms. This is shorter than the usual repetition rate, limited by the spin lattice relaxation time,

T_1, which at low temperatures is around 5–10 ms. The card provides 21 digital output channels (with TTL logic), thus enabling the control of a large number of devices without the need for additional delay generators.

The spectrometer is controlled using the SpecMan4EPR software [37], to which the DEER capability has been added. Both mw sources are controlled through the parallel LPT port. The magnet, the RF parts, data acquisition electronic and the probehead have not been changed [34].

4. Results

Fig. 2 presents the results of an inversion recovery nutation experiment, $t_p - t - 2\pi/3 - \tau - 2\pi/3 - \tau - echo$, carried out at 40 K on a sample of BDPA (α,γ-bisdiphenylene-β-phenyl allyl) in polyethylene. In this experiment the echo intensity is measured as a function t_p. It shows that the minimal duration of a π-pulse obtained when the power amplifier operates under saturation conditions is 25 ns. This corresponds to a nutation frequency of 20 MHz, as obtained from the FT of the time domain data, Fig. 2b. The quality factor, Q, of the loaded cavity is ∼1000 and the cavity bandwidth is ∼100 MHz at this temperature.

The relationship between the incident power P and the energy stored in the cavity for a critically coupled cavity is: [38]

$$P = \frac{\omega_0}{\mu_0 Q} V_{cav} \langle B_1^2 \rangle_{cav}, \tag{1}$$

where ω_0 is the frequency, V_{cav} is the cavity volume and $\langle B_1^2 \rangle_{cav}$ is the average microwave field in the cavity. For the TE_{011} cylindrical

Table 1
List of the W-band mw components of the bridge and their major specifications

Component	Company/cat. number	Bandwidth	Insertion loss	Other details
Narrow band amplifier	Quinstar IS-10/95	±500 MHz		Gain = 16 dB
PIN phase Modulator	Quinstar FPM-10-95-180	±250 MHz	3 dB	Switching time 5 ns
Power amplifier	Quinstar QPP-94043025	92–96 GHz		1 Watt, 23 dB gain
Variable PIN Attenuator	Quinstar QSA-95200W	±1 GHz	3.0 dB	0-20 dB
PIN switch	ELVA1 SPST-10/95/2	±1 GHz	2.0	Switching time 5 ns, isolation 60 dB
Frequency multiplier	ELVA1 IAFM-10/95/13	±250 MHz		Output power 13 dbm (20 mW)
Directional coupler	Hitachi QJG-W03300		2.5 dB	3 dB directivity
Isolator	ELVA1 IS-10/95	±1 GHz	0.5 dB	25 dB
Directional coupler	Quinstar QJG-W20300	75–110 GHz	1.4 dB	25 dB directivity
Precision junction circulator	Quinstar QJY-95013 W	94.5-95.5 GHz	1.6 dB	35 dB
W-band zero biased detector	ELVA1 ZBD-10	75–110 GHz		
Manual phase shifter	Quinstar QDP-W0000	75–110 GHz	0.3 dB	0–180°
Low noise amplifier	Quinstar QLN-95106028-I2	1 GHz		Gain 28 dB, noise figure 6 dB
Narrow band amplifier	Quinstar QPN-95011816-I2	94.5–95.5 GHz		Gain = 16 dB, output power 18 dbm (63.1 mW)
Mixer	Spacek M95-U	94–96 GHz		Conversion loss 6 dB
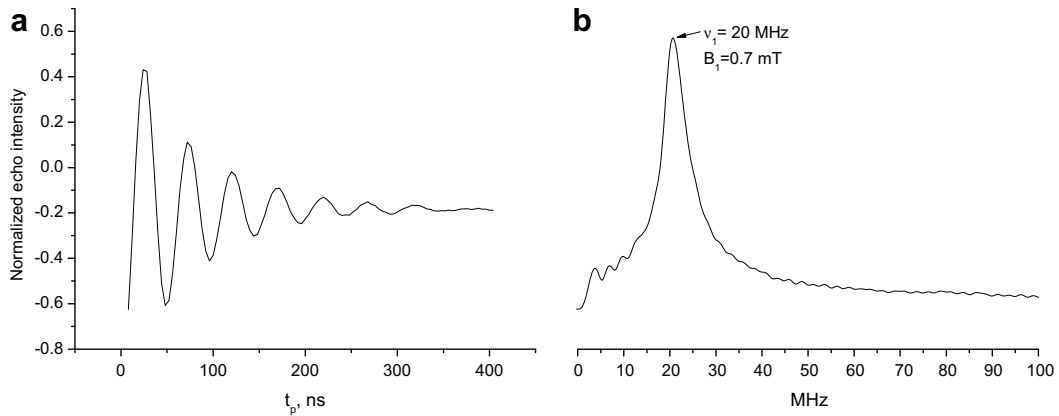
Fig. 2. Measurements of the Rabi-oscillations on a BDPA/polystyrene using the inversion recovery sequence ($t_p - t - 2\pi/3 - \tau - 2\pi/3 - \tau - echo$), where the echo intensity is measured as a function of t_p. The durations of the $2\pi/3$ pulse was 20 ns, $t = 1$ μs, $\tau = 400$ ns, $T = 40$ K. (a) The time domain data. (b) The corresponding Fourier transform.

cavity mode, the average magnetic field over the cavity volume is related to the magnetic field that is felt by a small sample in the center of the cavity, $\langle B_1^2 \rangle_s$, according to: [38]

$$\langle B_1^2 \rangle_{cav} = 0.0811(1 + (0.82a/d)^2)\langle B_1^2 \rangle_s, \tag{2}$$

where a is the cavity height and d is its diameter. Accordingly, Eq. (1) can be rewritten as:

$$P = \frac{\omega_0}{\mu_0 Q}\langle B_1^2 \rangle_s 0.0811(1 + (0.82a/d)^2)V_{cav} \tag{3}$$

The length of a π pulse is:

$$t_p = \frac{\pi}{\gamma_e \sqrt{\langle B_1^2 \rangle_s}} \tag{4}$$

and using Eqs. (3 and 4) one obtains:

$$t_p \text{ (ns)} = 1.26 \cdot 10^3 \sqrt{\frac{\nu_0 \text{ (GHz)}V_{eff} \text{ (cm}^3)}{P(W)Q}}, \tag{5}$$

where $V_{eff} = 0.0811 \cdot (1 + (0.82a/d)^2)V_{cav}$. For $a = 3$ mm and $d = 4.2$ mm $V_{cav} \sim 0.04$ cm^3 and $V_{eff} \sim 0.004$ cm^3. Thus, for a power level of 0.4 W, $Q \sim 1000$ and $\nu_0 = 95$ GHz, this yields $t_p \sim 26$ ns, in agreement with the experimental value. In our earlier set-up we estimated the incident power at the cavity as 120 mW [34], therefore for the same Q we expect a reduction by a factor of two in the length of the π pulse, yet we observe a factor of ~3. This could be due to a difference in Q (cavities have been changed over the years) and some overestimation of the incident power in the old system.

The deadtime of the spectrometer at room temperature, following a pulse of 50 ns at full power, is 50 ns, as shown in Fig. 3. This is comparable to the deadtime reported by Freed and coworkers [36]. Unfortunately, at low temperatures (<40 K) the deadtime increases

considerably to ~150 ns, which is too long. This can be probably reduced by modifying the coupling scheme of the probehead.

The issue of sensitivity in pulsed EPR has been discussed in detail in a number of publications [39,40], and it will not be repeated here. Nonetheless, in ESEEM and DEER applications, the sensitivity is determined not only by the S/N of the echo amplitude but by the modulation amplitude as well. Therefore, in the discussion of sensitivity we first refer to the usual situation where the characteristic width of the EPR spectrum exceeds the pulse bandwidth and the echo amplitude (and S/N ratio as well) increases proportionally to B_1. Therefore, the three fold increase of B_1 (as compared with our old W-band bridge) results in an approximately three fold increase in the signal amplitude for most applications, except Davies ENDOR which requires long selective pulses. Such an increase in signal amplitude is associated with a nine fold decrease of accumulation time, required to reach same S/N. Compared to most available W-band spectrometers with B_1 ~6–8 MHz, except for the unique Cornell spectrometer [36], which is not used for ESEEM investigations, this upgraded bridge offers a superior sensitivity in terms of echo amplitude.

As a simple demonstration of the sensitivity we prepared a solution of 0.5 mM 3 carboxy tempo in 1:1 water/glycerol. The solution was placed on a quartz tube of 0.6 i.d × 0.84 o.d and total sample volume was 1–2 µl. A two pulse echo generated with pulses of 12.5/25 ns ($\frac{\pi}{2}/\pi$) and $\tau = 300$ ns (40 K) had a $S/N = 13$ for a single shot. This implies that measurements of samples with nitroxide concentrations of ~0.04 mM exhibiting an echo amplitude with $S/N \sim 1$ per single shot, are realistic.

4.1. DEER measurements

DEER measurements were carried out on a rigid biradical, shown in Fig. 4a with a fixed distance of 3.6 nm between the two nitroxide [41,42,12]. The radical was dissolved in o-terphenyl, 0.5 mg/0.2 g, which corresponds to ~2.5 mM. The four pulse DEER was employed [43] (Fig. 4b) and the position of the pump (v_2) and observer (v_1) pulses are indicated on the echo-detected EPR powder pattern, shown Fig. 4c.

The time dependence of the echo intensity, $V(t)$, for the four pulse DEER experiment is: [44]

$$V(t) = V(0)\langle(1 - \lambda(1 - \cos \omega_{dd} t)\rangle \qquad (6)$$

$$\omega_{dd} = \frac{\mu_0}{4\pi\hbar} \frac{g_1 g_2 \beta^2}{r^3}(3\cos^2\theta - 1)$$

The distance between the two spins is r and θ is the angle between the external magnetic field $\vec{B}_0$ and the vector connecting the loci of
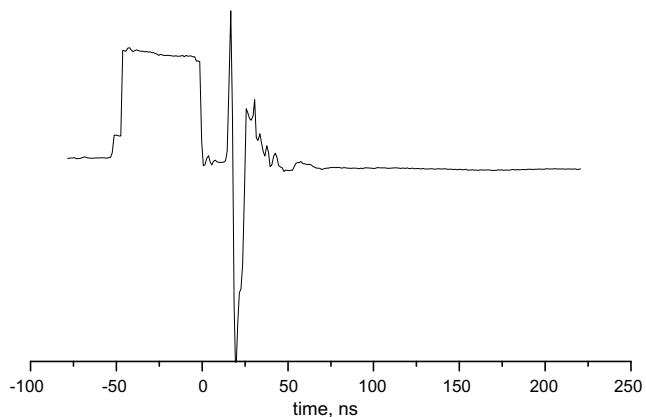

Fig. 3. A trace showing the noise obtained after the application of a 50 ns pulse at full power at room temperature.
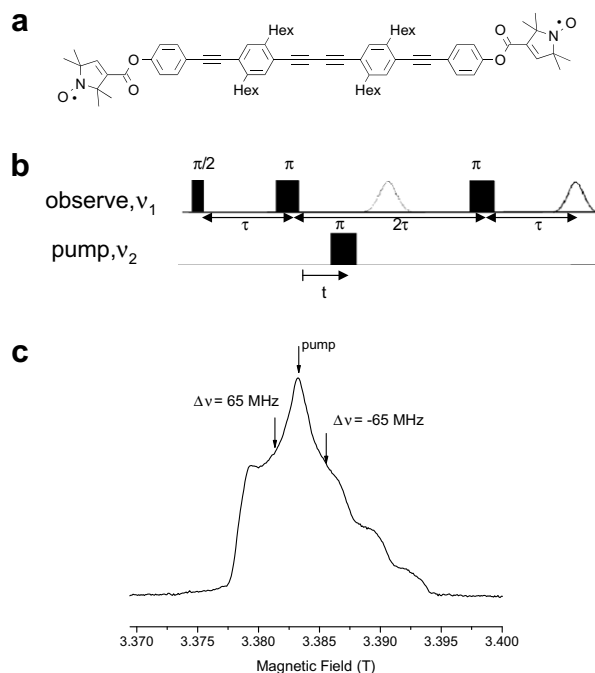

Fig. 4. (a) The biradical used in this work. (b) the four pulse DEER sequence. (c) the echo-detected EPR spectrum of the biradical recorded at 40 K with $t_{\pi/2} = 36$ ns, $t_\pi = 72$ ns and $\tau = 300$ ns. The arrows show the positions of the pump and observer pulses.

the two spins. For the specific radical studied, where r is fixed, the averaging in Eq. (6) should be carried out on θ only and the integration range depends on the position of the pump and observed pulses and the relative orientation of the g-tensors of the two nitroxide radicals [12] λ is the probability to flip one of the two spins by the pump pulse. When there is no correlation between the orientation of the g-tensors of the two spins, or when there is no orientation selection, the modulation depth, λ, is given by: [44]

$$\langle \lambda_k \rangle_{g(\Delta\omega_k)} = \int_{-\infty}^{\infty} \frac{\omega_1^2}{\omega_1^2 + \Delta\omega_k^2} \sin^2 \frac{(\omega_1^2 + \Delta\omega_k^2)^{1/2} t_p}{2} g(\Delta\omega_k) d\Delta\omega_k \qquad (7)$$

where ω_1 and t_p are the amplitude and duration of the pump π pulse, respectively, $\Delta\omega$ is the off-resonance frequency and $g(\Delta\omega_k)$ is the distribution function of $\Delta\omega$, which is given by the EPR spectrum. However, in the case of orientation selection and correlated orientations of the two radicals the modulation depth λ depends on the orientation selected by the observer and pump pulses and by the relative orientation of the g-tensors [9,10,12].

DEER measurements were carried out with two pulse settings. The first (a) was chosen to be the same as that used recently in W-band DEER measurements on a commercial Bruker spectrometer, with a power upgrade [12], with $t_p = 80$ ns and $t_{\pi/2}, t_\pi = 80/160$ ns for the observer pulses. For the second, (b), $t_p = 24$ ns and $t_{\pi/2}, t_\pi = 48/96$ ns. The latter represents the shortest π pulse that can be achieved with our current set-up and corresponds to $\lambda = 0.17$ as calculated from Eq. (7) using the powder lineshape given in Fig. 4c. The DEER trace recorded with settings (a) and $\Delta v = v_1 - v_2 = -65$ MHz is shown in Fig. 5A, trace a. Trace b was obtained with settings (b) and the same Δv. The difference in the modulation depth between the two traces is remarkable. Also the number of scans required for the long pulse measurement was considerably larger. Additional measurements were carried out with setting (b) but $\Delta v = 65$ MHz, trace c, to illustrate the effect of the orientation selection. Note the difference in modulation depth for the same pump pulse length and frequency. The data
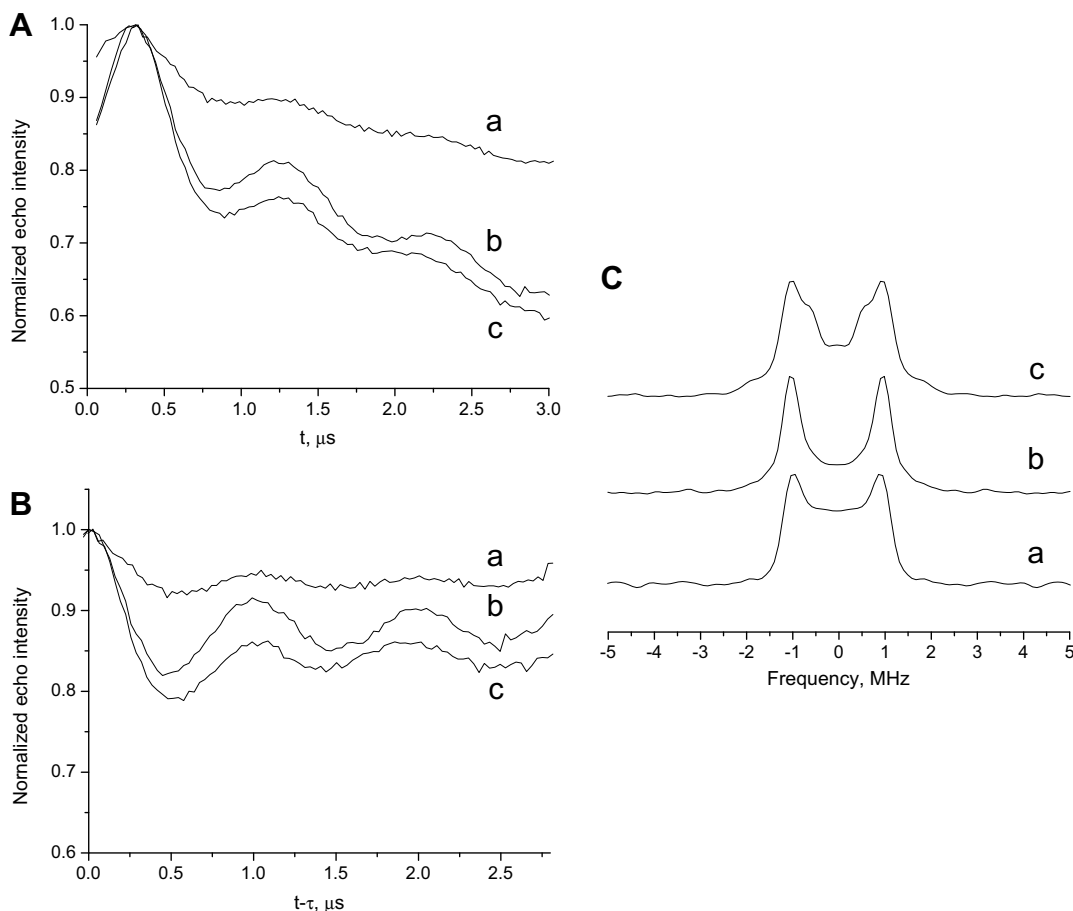
Fig. 5. (A) Four pulse DEER traces of the biradical (r = 3.6 nm) obtained with t_p = 80 ns, $t_{\pi/2}, t_\pi$ = 80/160 ns, Δv = −65 MHz (trace a, #scans = 142), t_p = 24 ns, $t_{\pi/2}, t_\pi$ = 48/96 ns, Δv = −65 MHz (trace b, #scans = 7), and Δv = 65 MHz (trace c, #scans = 15). All traces were obtained with 30 shots per scan, τ = 300 ns and T = 40 K. (B) The DEER data after background subtraction. (C). The corresponding Fourier transforms.

after removal of the background decay and shifting of the time scale to (t-τ) are shown in Fig. 5B and the corresponding Fourier transforms are given in Fig. 5C. Comparison of traces b and c in Fig. 5B shows that they have a different lineshape due to orientation selection [12]. These results confirm that the advantage of short pulses in terms of S/N is two fold, more spins can be detected thus increasing the echo intensity and more spins can be pumped, increasing the modulation depth. The S/N of the traces shown in Fig. 5B indicates that an accumulation time of 12 h will be required to achieve the same S/N for a 0.2 mM sample. This shows that the accumulations times for biological samples with low concentrations are still reasonable.

4.2. HYSCORE measurements

HYSCORE measurements were carried out on a NO bound ferrous myoglobin complex, which was obtained by reducing ferric myoglobin with ascorbate in the presence of nitrite. The sample used had 5 mM myoglobin in 50 mM sodium phosphate buffer. The W-band echo detected spectrum of the resulting complex, recorded at 8 K, is depicted in Fig. 6a. It shows the presence of two types of NO bound myoglobins as reported earlier [45,46]. One with an axial g- tensor ($g_\perp$ = 2.030, $g_\parallel$ = 1.981) and the other with a rhombic g-tensor (g_{xx} = 2.075, g_{yy} = 1.987, g_{zz} = 2.008). Measurements were carried out at the single-crystal like g_{xx} position (g = 2.074, B_0 = 3.27 T) of the rhombic complex, where there is no contribution from the axial complex. The pulse sequence employed was $\pi/2$-τ-$\pi/2$-t_1-π-t_2-$\pi/2$-τ-$echo$ [47] with $\pi/2$ and π pulses of 12.5/25 ns respectively. A four step phase cycle was employed to

remove unwanted echoes [48]. The HYSCORE spectrum is depicted in Fig. 6b. The (+,+) quadrant shows peaks at (17.3, 1.6) MHz and (19.3, 3.4) MHz that are assigned to single quantum-single quantum (ss) correlations of the coordinated ^{14}N nucleus of the axial histidine ligand [49]. It shows an additional single quantum-double quantum (sd) correlation at (17.3, 5.0) MHz and a double quantum - double quantum (dd) correlation at (36.8,5.0) MHz. These cross-peaks allowed us to determine all six ENDOR frequencies of this nucleus at this single crystal-like field orientation for the two electron spin manifolds; (17.3, 19.3, 36.7) MHz and (1.6, 3.4, 5.0) MHz. The first order expressions for the single quantum ENDOR frequencies in the two electron–spin manifolds, $v_{sq_{1,2}}^{\pm}$, are: [50].

$$
\begin{aligned}
v_{sq_1}^{\pm} &= \frac{1}{2}A \pm v_I + \frac{3}{2}Q \\
v_{sq_2}^{\pm} &= \frac{1}{2}A \pm v_I - \frac{3}{2}Q
\end{aligned}
\tag{8}
$$

where v_I is the nuclear Larmor frequency, A is the hyperfine coupling and Q is the quadrupolar coupling at this particular orientation. Using these expressions we obtained for the g_{xx} position A(His) = 15.8 MHz and Q(His) ≈ 0.6 MHz. The modulation depth of this nucleus is large (up to 20% in the three-pulse ESEEM experiment) because A is close the cancellation condition ($A \sim 2v_I$).

Weak peaks corresponding to the heme ^{14}N can also be observed at the (+,+) quadrant at (9,13) MHz. These yield an estimated hyperfine coupling of about 4 MHz. The peaks at the (−,+) quadrants are due to the ^{14}N of the NO ligand and they appear at (24.6, 5.7) MHz and (27.9, 10.4) MHz and correspond to two ss cor-
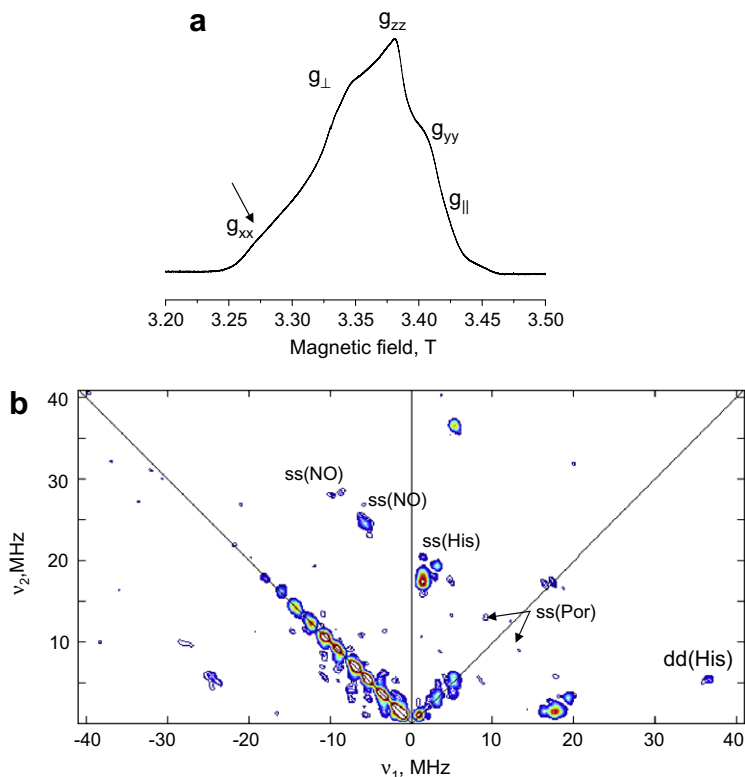
Fig. 6. (a) The echo-detected EPR spectrum of myglobin-NO. (b) A HYSCORE spectrum of myglobin-NO recorded at $g = 2.074$ (indicated by an arrow on the EPR spectrum). The pulses used were $t_{\pi/2} = 12.5$ ns, $t_\pi = 25$ ns, $\tau = 260$ ns and the dwell time in t_1 and t_2 was 12.5 ns. The starting value of t_1 and t_2 was 40 ns and 120×120 points were collected with 10 shots per point and one scan. The peaks are assigned on the Figure. The noise on the $(-,+)$ diagonal is due to incomplete removal of the unwanted echoes by the phase cycling.

relations. They appear in the $(-,+)$ quadrant because the hyperfine coupling is within the strong coupling regime. From these frequencies we estimate $A(\text{NO}) = 32.5$ MHz and $Q(\text{NO}) = 1.1–1.5$ MHz. These results show that systematic HYSCORE measurements along the EPR powder pattern can potentially resolve the ^{14}N histidine hyperfine and quadrupole interactions of the axial and rhombic species. Such measurements are currently underway and will be reported later.

HYSCORE measurements were also carried out on $V^{17}O(H_2^{17}O)_5^{2+}$ in a frozen solution of water/glycerol obtained by dissolving VOSO$_4$ in 40% enriched H$_2^{17}$O. The spectrum, recorded at the $g_\perp$ region (maximum echo, 3.38 T), is shown in Fig. 7. Signals appeared only in the $(+,+)$ quadrant. The peak on diagonal at (20.6, 20.6) MHz, corresponding the ^{17}O Larmor frequency, is attributed to solvent water molecules. Two other signals are situated symmetrically with respect to the diagonal, the first at (18.2, 23.3) MHz and the second at (13.4, 28.4) MHz (measured at the center of the peak). These yield hyperfine couplings of 5 and 15 MHz, respectively. Here, unlike in the case of the ^{14}N signals described above, the modulation depth is very shallow ($\sim4\%$) because of the partial enrichment and the departure from the cancellation condition. Nonetheless, it was easy to obtain a high quality spectrum. ^{17}O frequencies at the same positions were observed earlier in the W-band ENDOR spectrum of this sample [51]. The doublet with the larger hyperfine coupling was assigned to the oxo oxygen, whereas the signal with the smaller coupling was assigned to the water ligands.

5. Conclusions

A W-band (95 GHz) microwave bridge with a simple and flexible design, based on commercially available microwave compo-
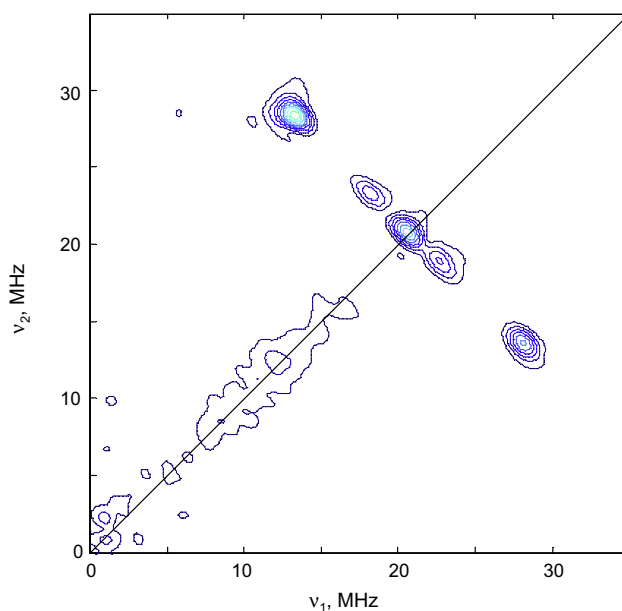
Fig. 7. A HYSCORE spectrum of VOSO$_4$ in a 1:1 water (40% H$_2^{17}$O)/glycerole solution recorded at $B_0 = 3.38$ T, $T = 20$ K and $t_{\pi/2} = 15$ ns, $t_\pi = 30$ ns, $\tau = 200$ ns and a dwell time of 15 ns in t_1 and t_2. The starting value of t_1 and t_2 was 30 ns, 80×80 points were collected with 30 shots per point and one scan.

nents, has been constructed and the performance of the spectrometer demonstrated. The short π pulses this bridge produces increase considerably the sensitivity of DEER measurements at high fields. Moreover, HYSCORE spectra could be measured,

allowing us to detect nuclear modulations from low γ nuclei such as ^{14}N and ^{17}O with nuclear frequencies as high as 40 MHz, spanning a 4–33 MHz range of hyperfine couplings. This opens a new window for the observations of relatively large hyperfine couplings that are not resolved in the EPR spectrum and are yet difficult to observe with conventional X-band ESEEM. Although such high frequencies may be observed by ENDOR experiments, the correlations provided by HYSCORE are most important for signal assignment and the high resolution provides quadrupolar splittings.

Acknowledgments

References

[1] O. Grinberg, L.J. Berliner (Eds.), Biological Magnetic Resonance, Vol. 22, Kluwer Plenum Publishers, New York, 2004.
[2] D. Goldfarb, Phys. Chem. Chem. Phys. 8 (2006) 2325–2343.
[3] K. Möbius, D. Goldfarb, in: Thijs Aartsma, Joerg Matysik (Eds.), Biophysics Techniques in Photosynthesis, Volume II, Springer, Netherlands, 2008, pp. 267–304.
[4] P.C. Riedi, G.M. Smith, Electron Paramagnetic Resonance, A Specialist Periodical Report, in: N.M. Atherton, M.J. Davies, B.C. Gilbert, K.A. McLauchlan (Eds.), The Royal Society of Chemistry, London, vol. 18, 2002, pp. 254–303.
[5] W. Lubitz, K. Möbius, K.-P. Dinse (Eds.), High-field EPR in Biology, Chemistry and Physics, Magnetic Resonance in Chemistry, Vol. 43, Wiley, London, 2005.
[6] K. Möbius, A. Savitsky, A. Schnegg, M. Plato, M. Fuhs, Phys. Chem. Chem. Phys. 7 (2005) 19–42.
[7] P.P. Borbat, J.H. Freed, Methods Enzymol. 423 (2007) 52–116.
[8] O. Schiemann, T.F. Prisner, Quart. Rev. Biophys. 40 (2007) 1–53.
[9] V.P. Denysenkov, T.F. Prisner, J. Stubbe, M. Bennati, Proc. Natl. Acad. Sci. 103 (2006) 13386–13390.
[10] V.P. Denysenkov, D. Biglino, W. Lubitz, T.F. Prisner, M. Bennati, Angew. Chem. Intl. Ed. 47 (2008) 1224–1227.
[11] A. Savitsky, A.A. Dubinskii, M. Flores, W. Lubitz, K. Möbius, J. Phys. Chem. B 111 (2007) 6245–6262.
[12] Y. Polyhach, A. Godt, C. Bauer, G. Jeschke, J. Magn. Reson. 185 (2007) 118–129.
[13] A. Schweiger, G. Jeschke, Principles of Pulse Electron Paramagnetic Resonance, University Press, Oxford, 2001.
[14] A. Dikanov, Y.D. Tsvetkov, Electron Spin Echo Envelope Modulation (ESEEM) Spectroscopy, CRC press, Boca Raton, 1992.
[15] A.V. Astashkin, C. Feng, A.M. Raitsimring, J.H. Enemark, J. Am. Chem. Soc. 127 (2005) 502–503.
[16] K. Matar, D. Goldfarb, J. Magn. Reson. A 111 (1994) 50–56.
[17] A.M. Tyryshkin, S.A. Dikanov, D. Goldfarb, J. Mag. Reson. A 105 (1993) 271–283.
[18] R.B. Clarkson, D.R. Brown, J.B. Cornelius, H.C. Crookham, W.J. Shi, R.L. Belford, Pure Appl. Chem. 64 (6) (1992) 893–902.
[19] A.V. Astashkin, A.M. Raitsimring, F.A. Walker, Chem. Phys. Lett. 306 (1999) 9–17.
[20] J.H. Hankiewitcz, C. Stenland, L. Kevan, Rev. Sci. Inst. 64 (1993) 2850–2856.
[21] M. Willer, J. Forrer, J. Keller, S. Van Doorslaer, A. Schweiger, R. Schuhmann, T. Weiland, Rev. Sci. Inst. 71 (2000) 2807–2817.
[22] S.A. Dikanov, A.M. Tyryshkin, I. Felli, E.J. Reijerse, J. Hüttermann, J. Magn. Reson. B 108 (1995) 99–102.
[23] A. Silakov, E.J. Reijerse, S.P.J. Albracht, E.C. Hatchikian, W. Lubitz, J. Am. Chem. Soc. 129 (2007) 11447–11458.
[24] I. Gromov, J. Shane, J. Forrer, R. Rakhmatoullin, Y. Rozentzwaig, A. Schweiger, J. Magn. Reson. 149 (2001) 196–203.
[25] A.V. Astashkin, J.H. Enemark, A.M. Raitsimring, Concpt. Magn. Reson. 29B (2006) 125–136.
[26] J.W. A Coremans, O.G. Poluektov, E.J.J. Groenen, G.W. Canters, H. Nar, A. Messerschmidt, J. Am. Chem. Soc. 119 (1997) 4726–4731.
[27] A. Bloeß, K. Möbius, T.F. Prisner, J. Magn. Reson. 134 (1998) 30–35.
[28] T.F. Prisner, M. Rohrer, K. Möbius, Appl. Mag. Res. 7 (1994) 167–183.
[29] A. Raitsimring, D.H. Crepeau, J.H. Freed, J. Chem. Phys. 102 (1995) 8746–8762.
[30] G. Jeschke, A. Schweiger, J. Chem. Phys. 105 (1996) 2199–2211.
[31] G. Jeschke, R. Rakhmatoullin, A. Schweiger, J. Magn. Reson. 131 (1998) 261–271.
[32] J.A.J.M. Disselhorst, H. Vandermeer, O.G. Poluektov, J. Schmidt, J. Magn. Reson. A 115 (1995) 183–188.
[33] O. Burghaus, M. Rohrer, T. Götzinger, M. Plato, K. Möbius, Meas. Sci. Technol. 3 (1992) 765–774.
[34] I. Gromov, V. Krymov, P. Manikandan, D. Arieli, D. Goldfarb, J. Magn. Reson. 139 (1999) 8–17.
[35] T.F. Prisner, S. Un, R.G. Griffin, J. Israel, Chemistry, 32 (1992) 357–363.
[36] W. Hofbauer, K.A. Earle, C.R. Dunnam, J.K. Moscicki, J.H. Freed, Rev. Sci. Instrum. 75 (2004) 1194–1208.
[37] B. Epel, I. Gromov, S. Stoll, A. Schweiger, D. Goldfarb, Concpt. Magn. Reson. B 26 (2005) 36–45.
[38] C.P. Poole Jr., Electron Spin Resonance: A Comprehensive Treatise on Experimental Techniques, second ed., Dover (Ed.), 1996.
[39] C.E. Davoust, P.E. Doan, B. Hoffman, J. Magn. Reson. A119 (1996) 38–44.
[40] T.F. Prisner, Adv. Magn. Opt. Reson. 20 (1997) 245–299.
[41] A. Godt, C. Franzen, S. Veit, V. Enkelmann, M. Pannier, G. Jeschke, J. Org. Chem. 65 (2000) 7575–7582.
[42] A. Godt, M. Schulte, H. Zimmermann, G. Jeschke, Angew. Chem. 118 (2006) 7722–7726.
[43] M. Pannier, S. Veit, A. Godt, G. Jeschke, H.W. Spiess, J. Magn. Reson. 142 (2000) 331–340.
[44] K.M. Salikhov, S.A. Dzuba, A.M. Raitsimring, J. Magn. Reson. 42 (1981) 255–276.
[45] R.H. Morse, S.I. Chan, J. Biol. Chem. 255 (1980) 7876–7882.
[46] P.P. Schmidt, R. Kappl, J. Hüttermann, Appl. Mag. Reson. 21 (2001) 423–440.
[47] P. Höfer, A. Grupp, H. Nebenführ, M. Mehring, Chem. Phys. Lett. 132 (1986) 279–282.
[48] G. Gemperle, A. Aebli, A. Schweiger, R.R. Ernst, J. Magn. Reson. 88 (1990) 241–256.
[49] R. LoBrutto, Y.-H. Wei, R. Mascarenhas, C.P. Scholes, J. Biol. Chem. 258 (1983) 7437–7448.
[50] S.A. Dikanov, A.M. Tyryshkin, J. Hüttermann, R. Bogumil, H. Witzel, J. Am. Chem. Soc. 117 (1995) 4976–4986.
[51] D. Baute, D. Goldfarb, J. Phys. Chem. A 109 (2005) 7865–7871.